

Supporting Information

Sub-nanometer vacancy defects introduced on graphene by oxygen gas

Yasuhiro Yamada,^{*,†,‡} Kazumasa Murota,^{†,‡} Ryo Fujita,[†] Jungpil Kim,[†] Ayuko Watanabe,[†] Masashi Nakamura,[†] Satoshi Sato,[†] Kenji Hata,[‡] Peter Ercius,[§] Jim Ciston,[§] Cheng Yu Song,[§] Kwanpyo Kim,^{||} William Regan,^{||} Will Gannett,^{||} Alex Zettl.^{||}

[†] Department of Applied Chemistry and Biotechnology, Chiba University, 1-33 Yayoi, Inage, Chiba 263-8522, Japan

[‡] National Institute of Advanced Industrial Science and Technology, Tsukuba, Ibaraki 305-8561, Japan

[§] National Center for Electron Microscopy, Lawrence Berkeley National Laboratory, Berkeley, CA 94720, USA

^{||} Department of Physics, University of California at Berkeley, CA 94720, USA

S1. Experimental

S1.1 Transfer method of graphene from a copper foil to a TEM grid and conditions for HRTEM observation

Graphene covering one side of a copper foil was removed by the following method. An O-ring was attached to a glass plate, and graphene on the copper foil was attached to the O-ring (Figure S1a). Oxygen-plasma etching was conducted to remove graphene on one side of copper foil at oxygen gas flow rate of $50 \text{ cm}^3 \text{ min}^{-1}$ and 50 watt for 20 sec (PE-200 PLC Model, Plasma Etch, Inc.). Graphene on the copper foil was analyzed by Raman spectroscopy as explained in section S2.1 (Figure S2). For HRTEM observation, graphene on the copper foil was transferred to holey amorphous carbon films with gold frame (Quantifoil R2/2, SPI Supplies/Structure Probe Inc.) by removing copper in ammonium persulphate aqueous solution (Figure S3).

HRTEM observations of the defective structure of graphene was carried out using the TEAM 0.5 aberration-corrected TEM.³² The microscope was operated in monochromated mode at 80 keV and tuned for bright atom contrast at positive defocus ($C_3 = \text{ca. } -11 \text{ } \mu\text{m}$, $C_5 = \text{ca. } 3 \text{ mm}$). The resulting electron dose rate was $\text{ca. } 5 \times 10^5 \text{ (electrons/sec} \cdot \text{nm}^2)$. Only eleven images were collected at different defocuses to minimize the total amount of electron dose. Graphene on the copper foil was analyzed by Raman spectroscopy (inVia Raman Microscope, Reinshaw PLC, laser wavelength; 633 nm).

S1.2 SWCNTs

SWCNTs prepared by super-growth method³⁴ were used as a substitute of graphene to obtain the Raman spectra, because holey amorphous carbon sheets covered on gold TEM grids was severely oxidized and the amorphous carbon sheets

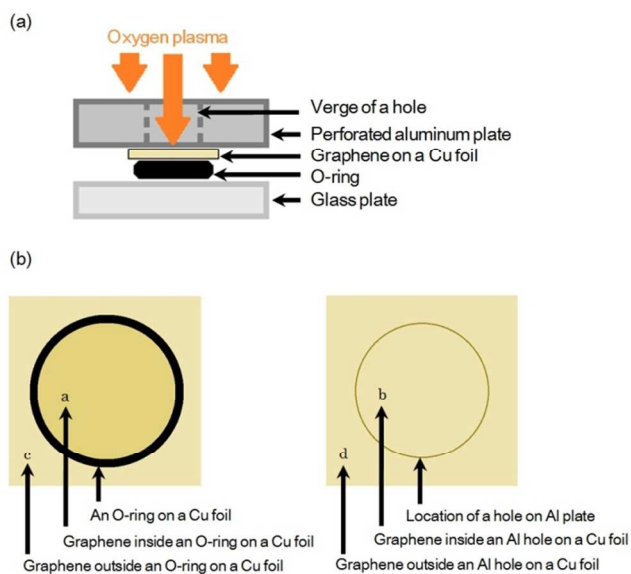


Figure S1. Setup for oxygen-plasma etching of graphene on a copper foil using an O-ring and a perforated aluminum plate. (a) A side view after being assembled. (b) Location of graphene exposed to and protected from the oxygen plasma used for Raman spectroscopy and HRTEM observation. The alphabets in (b) correspond to the positions for Raman spectra in Figure S2.

could not support graphene. The SWCNTs were utilized as alternatives because of the small curvature originating from the large diameter (ca. 3 nm), the high Brunauer-Emmett-Teller (BET) specific surface area ($1190 \text{ m}^2 \text{ g}^{-1}$ without opening the end caps) which is close to the BET specific surface area of one side of one layer graphene, and high purity compared

to the conventional SWCNTs. Oxidation of SWCNTs was carried out in a tube furnace under an oxygen gas flow rate of $5 \text{ cm}^3 \text{ min}^{-1}$ at 533 and 573 K for 168 h.

S1.3 Graphite

High purity graphite powder (SP-270, BET specific surface area = $265 \text{ m}^2 \text{ g}^{-1}$, Particle size = ca. $4 \mu\text{m}$, ash < 0.3 wt.%, Nippon Graphite Industries Ltd.) was used as a substitute of graphene because of the difficulty of analyses of single-layer graphene by XPS and elemental analysis. Oxidation of graphite was carried out in a tube furnace under oxygen gas flow rate of $5 \text{ cm}^3 \text{ min}^{-1}$ at 493, 553, and 573 K for 5 and 24 h. Oxygen contents of oxidized graphite were analyzed by elemental analysis (CE-440F, Elemental Analysis Inc.) and XPS (AXIS ULTRA DLD, Shimadzu Corp.). XPS was conducted using X-ray gun of Mg at 10 mA and 10 kV and pass energy of 40 eV. Samples were placed on conductive tapes (3M X-7001) for XPS analysis. In addition to the neutralization of samples during analysis, gold nano powder (99.9%, <100nm, Sigma-Aldrich Corp.) were placed on samples for correcting charging phenomenon. $\text{Au}_{4f_{7/2}}$ was set at 83.8 eV, and all of the spectra were adjusted. Modified asymmetric Voigt-type line-shapes⁵¹ were used to separate the waveform of XPS spectra. The maximum intensities of C_{1s} spectra were adjusted to 1.0 and intensities of O_{1s} were multiplied with the same number to adjust the intensity of C_{1s} spectra to be 1.0. Assignments of O_{1s} spectra were conducted by following our methods using density functional theory calculations.³⁸

S1.4 Conditions for calculations

Optimization of modeled structures was conducted by DFT calculation using B3LYP/6-31g(d) integral=grid=ultrafine of Gaussian 03.³³ The optimized structures were used for simulated HRTEM images by MactempasX (Total Resolution LLC) with parameters to match the TEAM 0.5 instrument.

The knock-on damage in graphene under electron beam has been reported to be related to lattice vibration as well as thermal effects,⁵² indicating that the accumulated energy applied on graphene by electron irradiation can be evaluated by calculating activation energy. Thus, stability of the optimized structures was evaluated by activation energies upon basically oxygen migration which were calculated from the difference between the total electron energy of optimized structures and that of the structures at transition states using Gaussian 03.

S2. Results and discussion

S2.1 Graphene

Pristine graphene was successfully transferred onto TEM grids without using a conventional polymer-coating method³¹ (Figures S3). More than one third of holes of amorphous carbon films was covered by graphene (Figure S3b), although there are wrinkles of graphene (Figure S3a). The fast Fourier transform mapping showed hexagonal spots (Figure S3a)³⁵ and the intensity ratio of I_{2D}/I_G of the spectrum was ca. 6 (Figures S2),³⁶ indicating that graphene prepared in this work is single-layered graphene.

After heat treatment in oxygen gas flow at 533 K for 24 h, the holey amorphous carbon films on TEM grids could not support oxidized graphene because of severe damage of holey carbon films by oxidation. Amorphous carbon films heated above 553 K for longer than 5 h (not shown) were also severely damaged. Thus, only samples heated at 533 K or lower for 5 h were used for HRTEM observation.

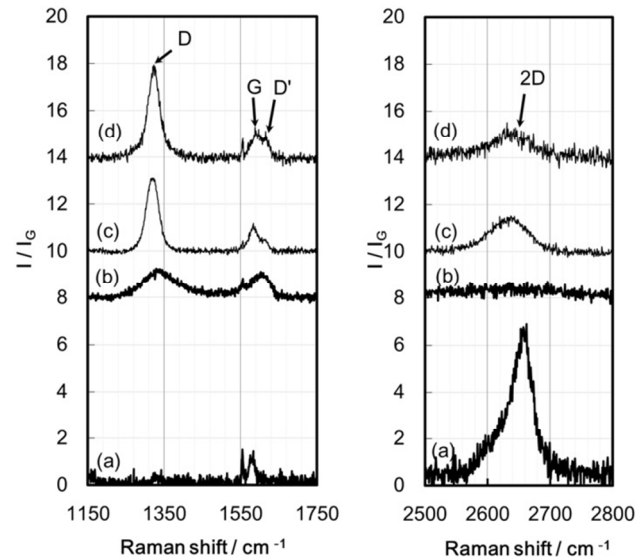


Figure S2. Raman spectra of graphene treated with oxygen plasma on copper foils. (a) Graphene inside the O-ring. (b) Graphene inside holes of the perforated aluminum plate. (c) Graphene outside the O-ring. (d) Graphene outside holes of the perforated aluminum plate. These alphabets in parentheses correspond to the positions at the alphabets in Figure S1.

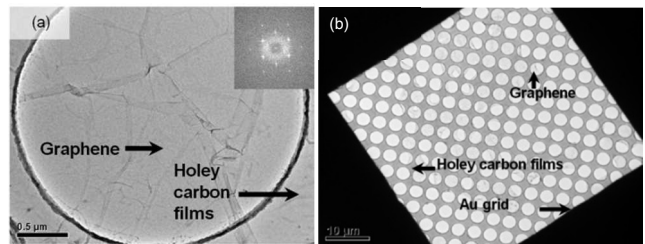


Figure S3. TEM images of graphene heated in vacuum at 773 K on holey amorphous carbon films of Au TEM grid. (a) At low magnification. (b) At the lowest magnification. The inset of (a) shows a Fourier transform of the magnified image.

Figure S2a and c shows Raman spectra of graphene inside and outside the O-ring (spots a and c in Figure S1b), respectively. Figure S2b and d shows Raman spectra of graphene inside and outside the hole of perforated aluminum plate (spots b and d in Figure S1b), respectively. The intensity ratio of I_D/I_G of the spectrum of graphene inside the O-ring was negligibly small (Figure S2a), whereas those of graphene outside the O-ring (Figure S2b) and graphene inside and outside the hole of perforated aluminum plate (Figure S2b and d) were higher than 1, indicating that these regions were severe-

ly damaged by oxygen plasma. The intensity ratio of I_{2D}/I_G has been utilized to distinguish the number of layers of graphene,^{15,30,36,53,54} where 2D originates the second order of zone-boundary phonons.³⁶ Intensity ratios of I_{2D}/I_G and I_G/I_D have been reported to be lowered by oxidation.¹⁵ This tendency was also observed for graphene outside the O-ring (a spot “c” in Figure S1b) and graphene inside and outside the hole of the perforated aluminum plate (spots “b” and “d” in Figure S1b). The peak of the 2D band of the spectrum was completely eliminated (Figure S2b), indicating that graphene was absent. Thus, the O-ring could protect graphene from the damage by oxygen plasma and only the region of graphene inside the O-ring was used for the reaction with oxygen gas.

S2.2 SWCNTs

Figure 2 shows the reactivity of the walls of SWCNTs analyzed by Raman spectroscopy. The reaction time of 168 h was selected to show the clear difference from pristine SWCNTs. The intensity ratio of I_D/I_G increased from 0.17 to 0.53 and the peak top of D band shifted from 1337 to 1345 cm^{-1} with increasing temperature from room temperature to 573 K. The peak at 1337 cm^{-1} originating from carbonaceous compounds on SWCNTs⁷ was removed, and the peak at 1345 cm^{-1} originating from vacancy defects with oxygen-containing functional groups was emerged at 573 K instead. The intensity of D' band originating from a double resonance Raman feature induced by disorder and defects^{21,22,24} has been reported to be a measure of boundary-like defects, vacancy-type defects, and sp^3 type defects by comparing with the intensity of D band.²⁴ As the oxidation temperature increased, the intensity ratio of $I_{D'}/I_D$ also increased, where the Raman shift of $I_{D'}$ is at ca. 1620 cm^{-1} . The intensity ratio of $I_{D'}/I_D$ at 573 K was ca. 5 in this work, which is close to boundary-like defects ($I_{D'}/I_D \sim 3.5$) and vacancy-type defects ($I_{D'}/I_D \sim 7$) rather than sp^3 -type defects ($I_{D'}/I_D \sim 13$).²⁴ From the increment of the intensity ratio of $I_{D'}/I_D$, it was indirectly shown that vacancy defects were introduced on the walls of SWCNTs at 533 and 573 K.

S2.3 Graphite

Table S1 shows the oxygen contents of oxidized graphite analyzed by elemental analysis. As the temperature increased from 493 to 573 K and the time of reaction increased from 5 to 24 h, the oxygen contents increased. The maximum oxygen content was 1.7 wt.% at 573 K for 24 h. This result shows that the reaction of graphite with oxygen gas starts below 493 K. Assuming that all of the edges of graphite with particle size of 4 μm were reacted and terminated with oxygen atoms, the maximum oxygen contents in graphite ($O/(C+O)$) is 0.014 wt.% by calculation, but the analyzed oxygen contents in graphite heated at 493 K for 5 h was 1.0 wt.%, indicating that the basal plane of the graphite was reacted.

Figure 3 shows O1s XPS difference spectra between graphite and graphite heated under oxygen gas flow at 493, 533, and 573 K for 5 h. At 493 K, Peak 2 at 532 eV corresponding to epoxides and unzipped epoxides^{18,20,38} as well as Peak 3 at 533.4 eV corresponding to pyran-like ether^{18,20,38} were formed. Because Peaks 2 and 3 increased at 493 K compared to as-

received graphite, oxygen is considered to be chemisorbed on the basal plane of graphene below 493 K. As the temperature increased, Peak 1 at 530.2 eV corresponding to C=O of quinone and lactone^{18,20,38} and Peak 3 corresponding to pyran-like ether and C-O-C in lactone increased. These functional groups have been theoretically^{17,19,38} and experimentally^{18-20,38} investigated as functional groups in the basal plane of graphite reacted with atomic oxygen using plasma after ion bombardment as well as functional groups in the basal plane of graphite oxide. Carbonyl groups and pyran-like ether have also been known as thermally stable functional groups which decompose above 973 K,⁵⁵ and it is no doubt that these functional groups are present on graphene in this work even after heat treatment at 773 K in vacuum. Presence of C=O of Peak 1 and pyran-like ether of Peak 3 indicates the scission of C-C bonding of graphene in the basal plane and formation of oxygen-containing functional groups and vacancy defects.^{17,20,38} The normalized intensity of Peak 1 increased from 0.002 to 0.004 as the temperature increased from 493 to 573 K. The normalized intensity of Peak 3 also increased from 0.01 to 0.025 as temperature increased from 493 to 573 K. Increment of Peaks 1 and 3 between 493 and 533 K is an evidence of formation of vacancy defects, whereas Peak 2 (epoxide and unzipped epoxide) is not an indication of vacancy defects because of the configurations of these functional groups. Thus, the range of reaction temperature between 493 and 533 K is the onset temperature to introduce vacancy defects in the basal plane of graphite from the results of XPS spectra.

Table S1. Oxygen contents of as-received graphite and graphite heated in oxygen gas.^{a)}

Treatment	C (wt.%)	O (wt.%)
As-received	99.1	0.0
O ₂ 493 K 5 h	98.1	1.0
O ₂ 533 K 5 h	97.9	1.2
O ₂ 573 K 5 h	97.5	1.6
O ₂ 493 K 24 h	97.8	1.3
O ₂ 533 K 24 h	97.7	1.4
O ₂ 573 K 24 h	97.4	1.7

^{a)} Ash content (0.3 wt.%) and nitrogen content (0.6 wt.%) for all samples) were subtracted.

S2.4 Simulated HRTEM images

Figure S4 shows an example of a simulated HRTEM image of graphene with pyran-like ether, C=O, and a dangling bond. This structure may not be present, but this structure was used to show the difference of in-plane and out-of plane atoms. An out-of-plane oxygen-containing functional group, which is C=O in Figure S4c, increased the brightness compared to other carbon atoms as indicated by Erickson et al.,²⁸ whereas in-plane oxygen-containing functional groups such as pyran-like ether and an in-plane carbon atom with a dangling bond had small difference in the brightness of the image. Increment of the brightness was also obtained for epoxide in the basal plane (Figure S5a4).

Other possible structures of Figure 4a1 and b1 are shown in Figure S5a2 and b2, and corresponding simulated images are

shown in Figure S5a4 and b4. These structures of the simulated images in Figure S5a2 and b2 were not selected as proposed structures in Figure 4 because of the poor similarities to the actual images (Figure S5a1 and b1) and the low stabilities of the simulated structures as explained in section 2.5. For example, the direction of the circled white spot corresponding to epoxide in Figure S5a4 was wrong compared to that of the corresponding white spot in Figure S5a1. Distance of circled C-C at a pentagon in Figure S5b4 is shorter than that of Figure S5b1.

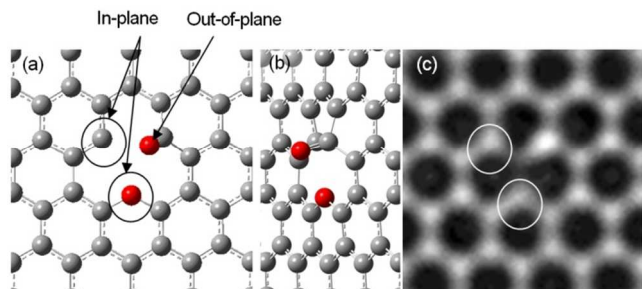


Figure S4. An example of a structure of graphene with pyran-like ether, C=O group, and dangling bond, and the corresponding simulated HRTEM image. (a) A modeled structure of graphene with an in-plane oxygen-containing functional group, an in-plane dangling bond, and an out-of-plane oxygen-containing functional group. (b) A perspective view of the structure (a). (c) The corresponding simulated HRTEM image. The pyran-like ether group and the dangling bond were circled in (a) and (c).

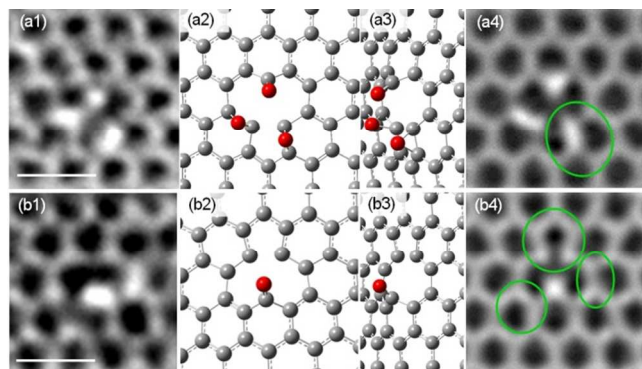


Figure S5. Phase images calculated by HRTEM exit wave reconstruction, examples of non-selected atomic structures, and corresponding simulated HRTEM images of graphene heated at 533 K for 5 h. These structures (a2 and b2) were not selected as proposed atomic structures. (a1 and b1) Reconstructed HRTEM phase images. These images are same as Figure 4a1 and b1. (a2 and b2) Examples of non-selected atomic structures with carbon atoms in gray and in-plane and out-of-plane oxygen-containing functional groups in red. (a3 and b3) Perspective views of (a2) and (b2). (a4 and b4) Simulated HRTEM phase images of (a2) and (b2). Green circles in (a4) and (b4) indicate the locations which look different from the actual image in (a1) and (b1). Scale bars are 0.5 nm.

S2.5 Stability of simulated structures

Stability of the proposed functional groups in Figure 4a2 and b2 was estimated by calculating activation energy (Figures S6 and S7). The activation energy required for migration of one oxygen atom from C=O at 4,5-position of a phenanthrene-like structure (Figure S6b1 and b2) was the lowest among those from all functional groups in Figure S6. This is probably because steric hindrance of two C=O groups increases the instability of the structure prior to the migration. Activation energies of most other functional groups were above 4.0 eV and energetically stable. The activation energy of the least stable functional groups in Figure S6 (2.5 eV) was higher than that of the highest activation energy of the most stable functional group in another estimated structure containing two epoxides and a C=O group (2.1 eV, Figure S8b5) in Figure S8. Thus, the structure in Figure 4a2 is proposed to be the structure in Figure 4a1, although the steric hindrance between functional groups exists.

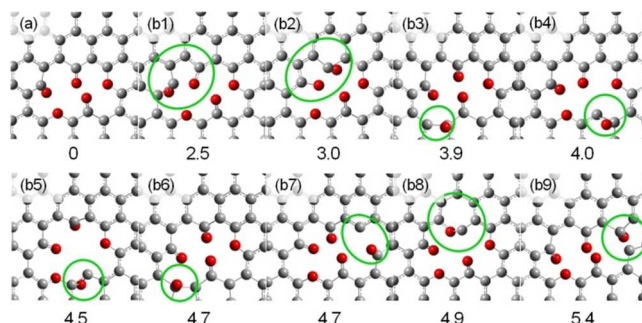


Figure S6. Activation energies to migrate one oxygen atom in the basal plane of the structure in Figure 4a2. (a) The structure in Figure 4a2. (b1-b9) Transition states. Green circles indicate the migrated oxygen atoms at different transition states. Activation energies in eV are written below each image.

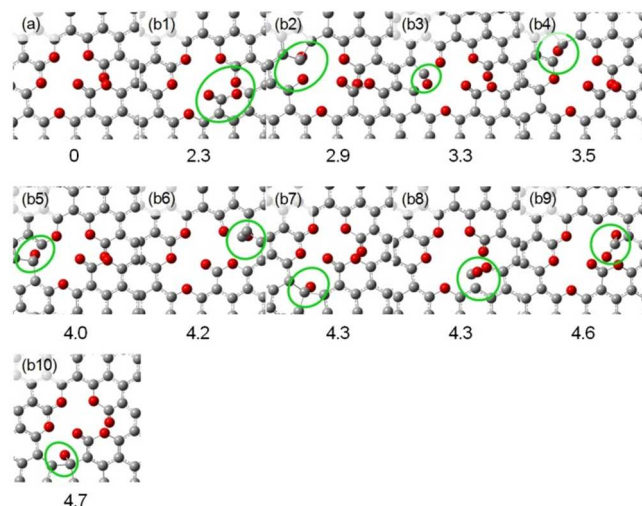


Figure S7. Activation energies to migrate one oxygen atom in the basal plane of the structure in Figure 4b2. (a) The structure in Figure 4b2. (b1-b10) Transition states. Green circles indicate the migrated oxygen atom at the transition state. Activation energies in eV are written below each image.

The activation energy required for migration of one oxygen atom from a lactone-like structure (Figure S7b1) was the lowest among functional groups in Figure S7 probably because steric hindrance of two lactone-like groups increases the instability of the structure prior to the migration and then formation of agglomerated pyran-like ether groups reduced the activation energy. Agglomerated pyran-like ether groups (Figure S7b2-5) have been reported as relatively unstable functional groups.³⁸ Thus, these functional groups showed relatively low activation energy (2.9 to 4.0 eV).

The lowest activation energy required for migration of one oxygen atom from another estimated structure with C=O and a point defect in Figure S9b1 (2.9 eV) was higher than that from the structure in Figure S7b1 (2.3 eV), but the similarity of the simulated HRTEM image of Figure 4b4 to the actual HRTEM image (Figure 4b1) was much higher than that of Figure S5b4. Thus, the structure in Figure 4b2 was selected as the estimated structure. We investigated other possible structures instead of Figures 4a2, 4b2, S5a2, and S5b2, but other possible structures were neither stable nor same appearance compared to the actual HRTEM images in Figure 4a1 and b1. Thus, presence of C=O, pyran-like ether, and lactone-like groups in Figure 4 can be explained from the viewpoints of HRTEM images as well as their stabilities.

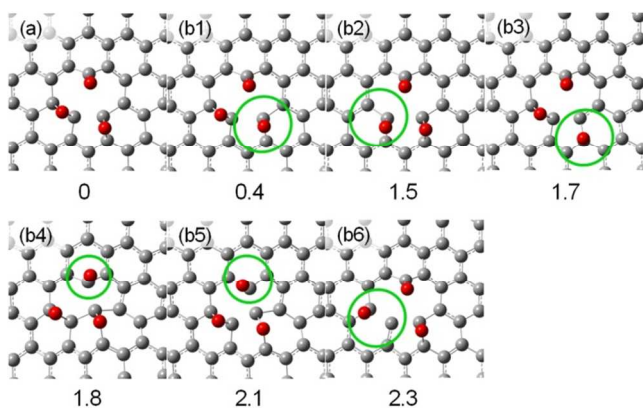


Figure S8. Activation energies to migrate one oxygen atom in the basal plane of the structure in Figure S5a2. (a) The structure in Figure S5a2. (b1-b5) Transition states. Green circles indicate migrated oxygen atoms at different transition states. Activation energies in eV are written below each image.

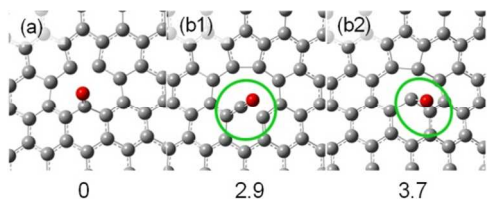


Figure S9. Activation energies to migrate one oxygen atom in the basal plane of the structure in Figure S5b2. (a) The structure in Figure S5b2. (b1,b2) Transition states. Green circles indicate migrated oxygen atoms at different transition states. Activation energies in eV are written below each image.

* Tel/Fax: +81-43-290-3376. E-mail address: y-yamada@faculty.chiba-u.jp (Y. Yamada).

Author Contributions

† These authors contributed equally.

REFERENCES

- (S1) Briggs, D.; Grant, J.T. Surface analysis by Auger and X-ray photoelectron spectroscopy. IMPublications and SurfaceSpectra Ltd.: West Sussex and Manchester, **2003**; pp 401-403.
- (S2) Meyer, J. C.; Eder, F.; Kurasch, S.; Skakalova, V.; Kotakoski, J.; Park, H.J.; Roth, S.; Chuvilin, A.; Eyhusen, S.; Benner, G.; Krasheninnikov, A. V.; Kaiser, U. *Phys. Rev. Lett.* **2012**, 108, 196102.
- (S3) Graf, D.; Molitor, F.; Ensslin, K.; Stampfer, C.; Hierold, C.; Wirtz, L. *Nano Lett.* **2007**, 7, 238-242.
- (S4) Ni, Z. H.; Wang, H. M.; Kasim, J.; Fan, H. M.; Yu, T.; Wu, Y. H.; Feng, Y. P.; Zhen, Z. X. *Nano Lett.* **2007**, 7, 2758-2763.
- (S5) Figueiredo, J.L.; Pereira, M. F. R.; Ereitas, M. M. M.; Orfao, J. J. M. *Carbon* **1999**, 37, 1379-1389.
